Monthly Notices
of the
ROYAL ASTRONOMICAL SOCIETY

Mon. Not. R. Astron. Soc. **426,** 2441–2451 (2012) doi:10.1111/j.1365-2966.2012.21429.x

Star formation in H I tails: HCG 92, HCG 100 and six interacting systems*

D. F. de Mello,[1,2]† F. Urrutia-Viscarra,[3] C. Mendes de Oliveira,[3] S. Torres-Flores,[4]
E. R. Carrasco[5] and E. Cypriano[3]

[1] *Physics Department, The Catholic University of America, Washington, DC 20064, USA*
[2] *Observational Cosmology Laboratory, Code 665, Goddard Space Flight Center, Greenbelt, MD 20771, USA*
[3] *Departamento de Astronomia, Instituto de Astronomia, Geofísica e Ciências Atmosféricas da USP, Rua do Matão 1226, Cidade Universitária, 05508-090, São Paulo, Brazil*
[4] *Departamento de Física, Universidad de La Serena, Av. Cisternas 1200 Norte, La Serena, Chile*
[5] *Gemini Observatory/AURA, Southern Operations Center, Casilla 603, La Serena, Chile*

Accepted 2012 May 31. Received 2012 May 4; in original form 2012 February 15

ABSTRACT

We present new Gemini spectra of 14 new objects found within the H I tails of Hickson Compact Groups (HCGs) 92 and 100. Nine of them are *Galaxy Evolution Explorer* (*GALEX*) far-ultraviolet (FUV) and near-ultraviolet (NUV) sources. The spectra confirm that these objects are members of the compact groups and have metallicities close to solar, with an average value of 12+log(O/H) $\sim$ 8.5. They have average FUV luminosities 7×10^{40} erg s^{-1} and very young ages (<100 Myr), and two of them resemble tidal dwarf galaxy (TDG) candidates. We suggest that they were created within gas clouds that were ejected during galaxy–galaxy interactions into the intergalactic medium, which would explain the high metallicities of the objects, inherited from the parent galaxies from which the gas originated. We conduct a search for similar objects in six interacting systems with extended H I tails: NGC 2623, NGC 3079, NGC 3359, NGC 3627, NGC 3718 and NGC 4656. We found 35 ultraviolet (UV) sources with ages < 100 Myr; however, most of them are on average less luminous/massive than the UV sources found around HCG 92 and HCG 100. We speculate that this might be an environmental effect and that compact groups of galaxies are more favourable to TDG formation than other interacting systems.

Key words: galaxies: interactions – intergalactic medium – galaxies: star clusters: general – galaxies: star formation.

1 INTRODUCTION

Interacting galaxies are ideal laboratories to probe galaxy evolution since tidal interaction is an important mechanism in shaping galaxy properties as we measure today. The H I gas, which is both the reservoir for star formation and an excellent tracer of the large-scale galaxy dynamics, is affected by tidal interaction and is often found in tails outside interacting galaxies. One of the key questions regarding the encounters of disc galaxies is the fate of the stripped H I gas. Do these H I intergalactic clouds form new stellar systems and/or dwarf galaxies known as tidal dwarf galaxies (TDGs)? And if they do, is there any difference in the types of objects that could be formed based on the type of environment where they are located? We have embarked in a series of papers trying to answer theses questions. In Torres-Flores et al. (2009), de Mello, Torres-Flores & Mendes de Oliveira (2008a) and Mendes de Oliveira et al. (2004, 2006), we showed that a few Hickson Compact Groups (HCGs) contain TDGs and intragroup star-forming regions. Other authors have also found TDGs and many young globular cluster candidates in compact groups (e.g. Gallagher et al. 2001; Iglesias-Páramo & Vílchez 2001). Other cases of intergalactic star-forming regions have also been reported outside interacting galaxies (e.g. Oosterloo et al. 2004; Ryan-Weber et al. 2004; Mullan et al. 2011; Werk et al. 2011), including young (<10 Myr) small stellar clusters in the H I

---

* Based on observations obtained at the Gemini Observatory, which is operated by the Association of Universities for Research in Astronomy, Inc., under a cooperative agreement with the National Science Foundation (NSF) on behalf of the Gemini partnership: the NSF (United States), the Science and Technology Facilities Council (United Kingdom), the National Research Council (Canada), CONICYT (Chile), the Australian Research Council (Australia), Ministério da Ciência e Tecnologia (Brazil) and Ministerio de Ciencia, Tecnologia e Innovacion Productiva (Argentina) – Observing run ID: GN-2003A-Q-53 and GN-2007B-Q-87.
†E-mail: demello@cua.edu

bridge between M81 and M82 (de Mello et al. 2008b) and outside the merger remnant NGC 2782 (Torres-Flores et al. 2012).

The importance of these newly formed objects as products of collisions is still debatable. They may be responsible for enriching the intragroup medium with metals which may have broad implications for galaxy chemodynamical evolution (Werk et al. 2011). They could grow to become independent objects as dwarf galaxies, or live as stellar clusters in the distant haloes of their hosts. In addition, one cannot exclude the possibility that they will dissolve and not remain gravitationally bound, yielding only very sparse star streams, or fall back on to the progenitor (Bournaud & Duc 2006).

The UV images of tidal tails, obtained with the *GALEX* satellite, showed UV-bright regions coincident with H I density enhancements (Hibbard et al. 2005; Neff et al. 2005). More recently, Thilker et al. (2009) reported the discovery of massive star formation in the Leo primordial H I ring which is having one of its first bursts of star formation. Therefore, UV and H I data together provide a powerful technique for identifying and studying star-forming regions in the vicinity of interacting galaxies. In de Mello et al. (2008a), we presented a sample of 16 star-forming region candidates in the intergalactic medium surrounding HCG 100. Here we present the optical data obtained with Gemini for HCG 100 and also for another compact group, HCG 92. We also present the UV data of six interacting galaxies with H I tails where we discovered 35 stellar cluster candidates.

This paper is organized as follows. Section 2 presents the data and results for HCG 92 and HCG 100; Section 3 presents the comparison sample and the discussion; Section 4 presents the summary, and the appendix (Section 4.1) describes the comparison sample in more detail. Throughout the paper, we assumed $\Omega_{\rm M} = 0.3$, $\Omega_\Lambda = 0.7$ and $H_0 = 100\,h$ km s^{-1} Mpc^{-1}, with $h = 0.71$.

2 HCG 92 AND HCG 100

The targets analysed here are the newly identified members of two HCGs of galaxies, HCG 92 and HCG 100 (Hickson 1982), located within their H I tails. HCG 92, known as Stephan's Quintet (e.g. Moles, Sulentic & Marquez 1997; Gallagher et al. 2001; Sulentic et al. 2001), is formed by three late-type galaxies (NGC 7318a, 7318b, 7319), one early-type (NGC 7317) at 80 Mpc and one object, NGC 7320, which is a foreground object. Mendes de Oliveira et al. (2004) presented the discovery of four intergalactic H II regions in the H I tail of HCG 92 located more than 25 kpc from the nearest group galaxy.

HCG 100 is formed by a bright central Sb galaxy (HCG 100a), an irregular galaxy with an optical tidal tail (HCG 100b), a late-type barred spiral (HCG 100c) and a late-type edge-on spiral (HCG 100d). It is the last group of Hickson's catalogue (1982) and is at 76.3 Mpc ($v_{\rm R} = 5336$ km s^{-1}). de Mello et al. (2008a) presented the *GALEX* far-ultraviolet (FUV) and near-ultraviolet (NUV) images of this group and identified 15 FUV sources located in the vicinity of the intergalactic H I clouds of the compact group which extends to over 130 kpc away from the main galaxies.

2.1 Spectroscopy with Gemini/GMOS

We have obtained new spectra of dozens of UV sources identified within the H I tails of HCG 92 and HCG 100, and derived their radial velocities. We also determined metallicities for those which turned out to be at the same redshift of the groups. Observations were performed with the Gemini Multi-Object Spectrograph (GMOS) at Gemini North in 2003 June (HCG 92) and in 2007 October and November (HCG 100). We centred GMOS slit on members of the groups and on sources which were identified in Mendes de Oliveira et al. (2004) and de Mello et al. (2008a). Other objects in the field were also observed when there was space left in the multislit mask. The spectra were obtained using the B600 and R400 gratings.

Exposure times for HCG 92 were 3 × 1500 s for the B600 grating and 3 × 1000 s for the R400 grating, covering from 3700 to 8000 Å. For HCG 100 data, the total exposure times were 3 × 600 s and 3 × 1200 s for the B600 and R400 gratings, respectively, and the final spectra covered a wavelength interval of 3700–7000 Å. Position angles were 20° and 300° from the usual orientation of GMOS; values for the airmass were 1.22 (R400) and 1.08 (B600) for HCG 92 and 1.03 for HCG 100, respectively. The seeing of 1 arcsec matched well with the slit size of 1 arcsec in both cases.

All spectra were biased, trimmed, flat fielded and wavelength calibrated with the Gemini IRAF package version 1.8 inside IRAF.[1] The final spectra have typical resolutions of 3.2 and 7.0 Å for the B600 and R400 gratings, respectively. The spectra of the regions in HCG 92 were not flux calibrated given that there were no standard calibrators observed around the time the data were taken. While the regions of HCG 100 had their flux calibrated using the spectrum of the stars BD+284211 (R400) and Hiltner 600 (B 600) observed in 2007 December 11. For reddening correction, we used the intrinsic Hα/Hβ ratio, with an intrinsic value taken by Osterbrock & Ferland (2006) for an effective temperature of 10 000 K and $N_{\rm e} = 10^2$.

We found 12 and 2 sources at the same redshift of HCG 92 and HCG 100, respectively. Four of the 12 sources had already been confirmed as members of HCG 92 by Mendes de Oliveira et al. (2004).

2.2 *GALEX* data

We obtained *GALEX* FUV and NUV background-subtracted images from the Multimission Archive at the Space Telescope Science Institute (MAST) and followed the method by de Mello et al. (2008a) to select UV sources within the H I tail or in the outskirts of the H I map. FUV and NUV fluxes were calculated using Morrisey et al. (2005) $m_\lambda = -2.5\log\,[F_\lambda/a_\lambda] + b_\lambda$. Fluxes were multiplied by the effective filter bandpass (FUV = 1528 ± 269 Å and NUV = 2271 ± 616 Å) to give units of erg s^{-1} cm^{-2}.

The *GALEX* fields of view are 1°.28 and 1°.24 in FUV and NUV, respectively, and the pixel scale is 1.5 arcsec pixel^{-1}. The images have a resolution full width at half-maximum (FWHM) of 4.2 and 5.3 arcsec in FUV and NUV, respectively. Despite the broad FWHM, *GALEX* is able to detect faint UV sources. The medium imaging survey, for instance, reaches $m = 24$ and 24.5 in FUV and NUV, respectively, with typical exposures of 1500 s (Bianchi et al. 2007). *GALEX* images have also been used extensively to search for very low surface brightness objects (e.g. Thilker et al. 2007) such as the ones we are interested in detecting. We chose the parameters to detect the UV with Source Extractor and perform photometry (SE, version 2.4.3; Bertin & Arnouts 1996) following the prescription of de Mello et al. (2008a,b) which was fine-tuned for detecting low surface brightness objects and clumpy systems. We matched both catalogues, FUV and NUV, within 3–4 arcsec radius. The SE's UV magnitudes (Mag_auto, AB system) were corrected for foreground Galactic extinction using $E(B-V)$ obtained from Schlegel,

---

[1] IRAF is distributed by the National Optical Astronomy Observatories, which are operated by the Association of Universities of Research in Astronomy, Inc., under cooperative agreement with the NSF.

Table 1. Star-forming regions in the H I tail of HCG 92 and HCG 100.

ID	ID_region	RA 2000	Dec. 2000	V (km s^{-1})	M_B [a] (mag)	12+log(O/H) O3N2	12+log(O/H) N2	Log(M_*)[b] (M$_\odot$)	Age[c] (Myr)	$L_{\rm FUV}$ (erg s^{-1})
HCG 92	1[d]	339.045 83	33.986 67	6615 ± 16	−12.30	8.44 ± 0.14	8.48 ± 0.18	4.2	$2.1\pm^{1}_{3}$[5.4]	40.74
	2[d]	339.062 50	33.984 17	6613 ± 59	−11.90	8.35 ± 0.14	8.45 ± 0.18	4.3	$2.2\pm^{2}_{5}$[4.1]	40.71
	3	339.058 33	33.967 50	6577 ± 69	−11.58	8.45 ± 0.14	8.55 ± 0.18	4.1	$2.4\pm^{7}_{2}$[5.5]	40.52
	4[d]	339.058 33	33.973 06	6659 ± 55	−12.10	8.48 ± 0.14	8.57 ± 0.18	5.7	$12.9\pm^{3}_{5}$[5.5]	40.50
	5	339.995 83	33.994 17	6035 ± 19	−11.34	8.40 ± 0.14	8.44 ± 0.18	7.6	$50.1\pm^{1}_{3}$[5.4]	41.30
	6	339.045 83	33.958 33	6543 ± 36	−12.57	–	8.69 ± 0.18	8.5	$100\pm^{5}_{3}$[6.4]	41.67
	7[d]	339.045 83	33.983 61	6612 ± 59	−12.69	8.32 ± 0.14	8.38 ± 0.18	7.9	$100\pm^{2}_{4}$[2.44]	41.06
	8	339.075 00	33.993 33	5628 ± 17	−13.23	8.50 ± 0.14	8.60 ± 0.18	–	...[7.6]	–
	9	338.975 00	33.953 89	5780 ± 12	−14.10	8.36 ± 0.14	8.48 ± 0.18	–	...[3.4]	–
	10	338.987 50	33.979 72	6020 ± 81	−15.25	8.62 ± 0.14	8.67 ± 0.18	–	...[5.3]	–
	11	339.045 83	33.982 78	6553 ± 52	−12.07	8.36 ± 0.14	8.47 ± 0.18	–	...[5.6]	–
	12	339.045 83	33.973 89	6621 ± 71	−9.88	8.46 ± 0.14	8.55 ± 0.18	–	...[3.9]	–
HCG 100	3[e]	0.270 83	13.023 33	5440 ± 61	−14.54	8.43 ± 0.14	8.43 ± 0.18	4.7	$1.0\pm^{-}_{-}$[6.1]	40.46
	4[e]	0.291 67	13.085 83	5337 ± 27	−13.42	8.42 ± 0.14	8.55 ± 0.18	4.7	$3.3\pm^{3}_{1}$[2.1]	40.51

[a] Calculated using magnitudes from Mendes de Oliveira et al. (2004) and de Mello et al. (2008a).

[b] Stellar mass (M$_\odot$) obtained from SB99 monochromatic luminosity, L_{1530} (erg s^{-1}Å^{-1}), for the ages given in column 9. Stellar mass (M$_\odot$) for H100-#3 and H100-#4 are from de Mello et al. (2008a).

[c] Age (Myr) estimated from the FUV−NUV colour. Values given in brackets: ages estimated from Hα equivalent width and SB99 models.

[d] The respective ID's in Mendes de Oliveira et al. (2004) for regions 1, 2, 4 and 7 in this table are d, a, b and c.

[e] ID from de Mello et al. (2008a).

Finkbeiner & Davis (1998), and $A_{\rm FUV} = E(B-V) \times 8.29$ and $A_{\rm NUV} = E(B-V) \times 8.18$ (Seibert et al. 2005). We used the Cortese et al. (2008) method for computing the internal extinction for each object in the FUV band. For each $A_{\rm FUV}$, we used the Seibert et al. (2005) extinction law, shown above, to obtain the $E(B-V)$.[2]

FUV and NUV colours were estimated using the task PHOT in IRAF, inside a fixed aperture of 4 or 5 arcsec radius, depending on the sizes of the sources, centred on the centroid of the light distribution of each NUV band detection.

2.3 Ages, masses and metallicities

We used the method described in de Mello et al. (2008a,b) to derive ages and masses from FUV and NUV *GALEX* images (Table 1). For each region, ages were estimated using the models given by STARBURST99 (SB99; Leitherer et al. 1999). These models were generated for an instantaneous burst, solar metallicity and Chabrier (2003) initial mass function (IMF), and are optimized for *GALEX* filter transmission curves. We have also generated models using Salpeter IMF and compared the results with Chabrier IMF. The difference in age between the two IMFs is around ∼2–4 Myr. In this paper, we are presenting only the results generated with Chabrier IMF. We have also included in Table 1 the errors for each age calculated from the errors in the colours.

We compared the ages determined spectroscopically by Mendes de Oliveira et al. (2004) with our values using *GALEX* and found an excellent agreement for three of the four regions (#1, # 2 and #4) for HCG 92. The object for which our age determination disagrees with respect to Mendes de Oliveira et al. (their region C and our region 7) is too close to another object, and *GALEX* is not able to resolve them. We have also estimated ages from the Hα equivalent widths and SB99 models (Table 1), and found agreement between the methods for four sources in HCG 92 and the two sources in HCG 100. However, three sources in HCG 92 are much older when calculated using the UV data than when using Hα. This could be due to the fact that UV light probes older stellar population than Hα and/or due to other factors including wrong correction for dust attenuation and positioning of the slit. We will discuss this later in this section when we compare our estimates with other authors. We cannot exclude the possibility that density-bounded conditions could produce lower equivalent widths, leading to apparent older ages when derived from them and SB99.

UV images showing the location of the newly detected members of HCG 92 and HCG 100 are shown in Figs 1 and 2. The Gemini optical image (filter *r*; Fig. 3) shows the peculiar and knotty morphology of the two UV sources in HCG 100 which resemble dwarf galaxies. They are located in the H I tail, and we suggest that they might be TDG candidates.

In Fig. 4, we show the spectra taken with gratings R400 and B600 for the two TDG candidates of HCG 100, and in Figs 5 and 6 we present two new star-forming regions of HCG 92, regions 3 and 5, which are similar to the four objects described in Mendes de Oliveira et al. (2004).

Metallicities of the regions were calculated using the empirical methods O3N2 and N2, proposed and calibrated by Pettini & Pagel (2004). These methods use line ratios [O III] λ5007/Hβ plus [N II] λ6584/Hα and [N II] λ6584/Hα, respectively, to estimate oxygen abundances. These estimators are adequate for faint extragalactic sources, such as the ones we are dealing with, because they are based only on very bright lines. The uncertainties on the calibration of these methods are 0.14 dex for O3N2 and 0.18 dex for N2 when 68 per cent of the points are included. Table 1 shows the estimated metallicities for the regions in HCG 92 and HCG 100, plus our new results on velocities (measured from the emission lines), masses and ages. As can be noted in Table 1, the metallicities derived from the O3N2 and N2 methods are in close agreement. For one of the regions of HCG 92 (region 6), we used only the N2 method due to the lack of Hβ.

---

[2] The values we find for $E(B-V)$ obtained from spectroscopy for regions 3 and 4 of HCG 100 are slightly different from the values calculated from the UV images. This difference could be due to the fact that the slit is not sampling the entire region and might be missing some of the regions where the UV flux originates. $E(B-V)$ values are: region 3 (0.10±0.01, 0.13) and region 4 (0.09±0.02, 0.05) – first value is from imaging and second value is from spectroscopy.

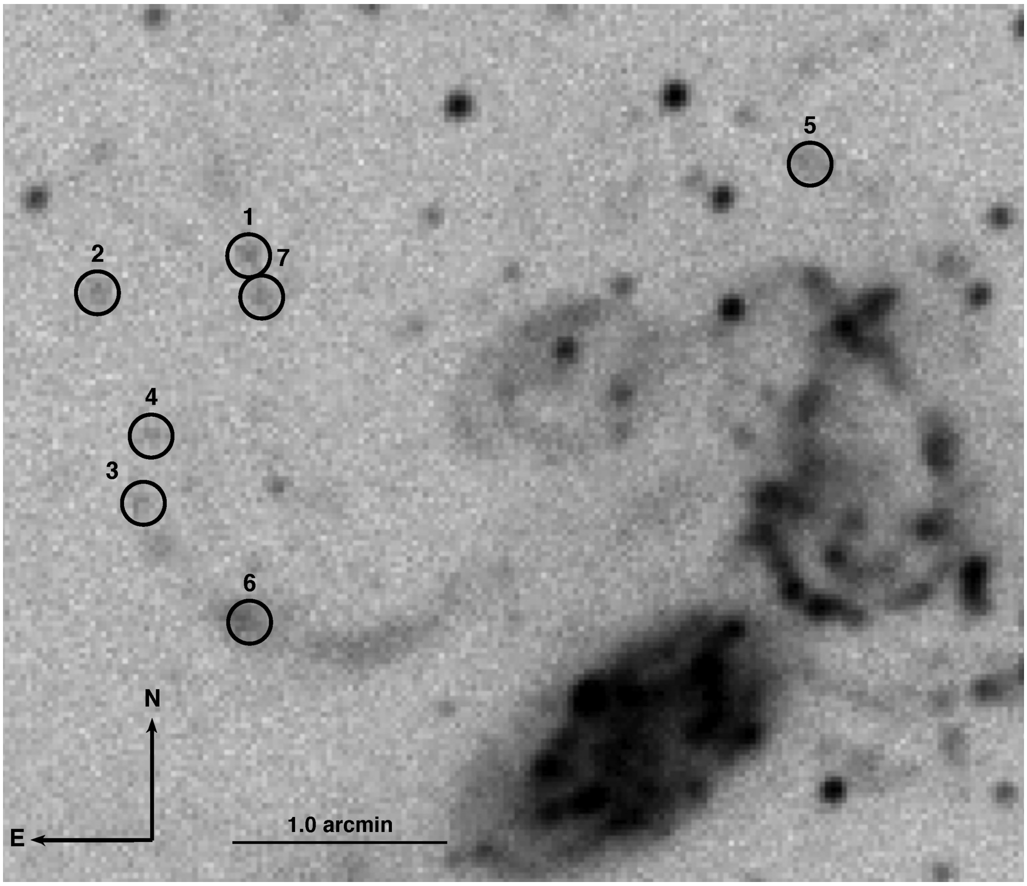

Figure 1. NUV image of HCG 92. Seven UV sources detected in the *GALEX* images are marked. North is up and East is to the left. Bar length is 1 arcmin.

We calculated line ratios and verified that all sources are star-forming regions as shown in the BPT diagnostic diagram (Baldwin, Phillip & Terlevich 1981) in Fig. 7. We plotted all Sloan sources from Kauffmann et al. (2003) for comparison.

In Fig. 8, we show our new data plotted on the metallicity–luminosity diagram (adapted from fig. 3 of Weilbacher, Duc & Alvensleben 2003). We estimated oxygen abundances using the method O3N2 described above. We also added new data from Croxall et al. (2009) to this figure. As expected, the main members of HCG 100 occupy the left-hand side of the diagram where luminous and metal-rich objects are located. Nearby dwarf irregular galaxies (Richer & McCall 1995) follow the well-known correlation indicated by the linear fit. Based on Fig. 8, all star-forming regions in the H I tail of HCG 92 and HCG 100 have metallicities similar to those of knots in tidal features, i.e. they have metallicities higher than those of local dwarf galaxies. Lisenfeld et al. (2008) and Mendes de Oliveira et al. (2004) found similar results for star-forming regions in the intergalactic medium of the systems Arp 94 and HCG 92, respectively.

Thus, we conclude that the metallicity measurements obtained here allowed us to distinguish between 'classical' dwarf galaxies and objects from tidal origin. We conclude that objects found within the H I tails of HCG 92 and HCG 100 were formed by pre-enriched material, and their metallicities are similar to or higher than that of their progenitor galaxies. It is also possible that their higher metallicities are due to a phenomenon called infant mortality (Fall, Chandar & Whitmore 2005) which destroys clusters by internal processes. In this way, the continuous star formation and destruction of stellar clusters could increase the metallicity of a given region after a few million years.

We have compared the coordinates of our targets with the ones identified in Trancho et al. (2012) using *Hubble Space Telescope* images and Gemini spectroscopy of HCG 92 and found no common sources. However, a close inspection of the *HST* images indicates that object T124 in Trancho et al. is the same as our object #6, but had wrong coordinates quoted in their paper. The H I tail is twice as long and has a different curvature than the optical tail; therefore, *HST's* small field of view did not cover the entire H I tail. The work by Trancho et al. (see also Fedotov et al. 2011) focused only on the optical tail, missing most of the targets we discovered. The age reported by those authors for T124 is in relative good agreement with the values we found for object #6 using the Gemini spectra (1.5 and 6 Myr, respectively). However, the age we found using the UV data, ∼100 Myr, is significantly higher. This disagreement can be explained, as pointed out in Trancho et al., by the fact that the slit did not cover the entire complex and is missing the other components of the clump. The UV data, on the other hand, cover the entire region and are more representative of the cluster. The UV is also known for detecting older stellar population than Hα and is a good age indicator for this type of stellar clusters. Therefore, our results suggest that T124 (or #6) is ∼100 Myr and $10^{8.5}$ $M_{\odot}$, making it the most massive TDG candidate in the outskirts of HCG 92. We have also inspected the location of this object with respect to the H I map (Mendes de Oliveira et al. 2004) and verified that it is located within one of the density peaks which support the idea that T124 (or #6) is a TDG candidate. According to Trancho et al., two other stellar

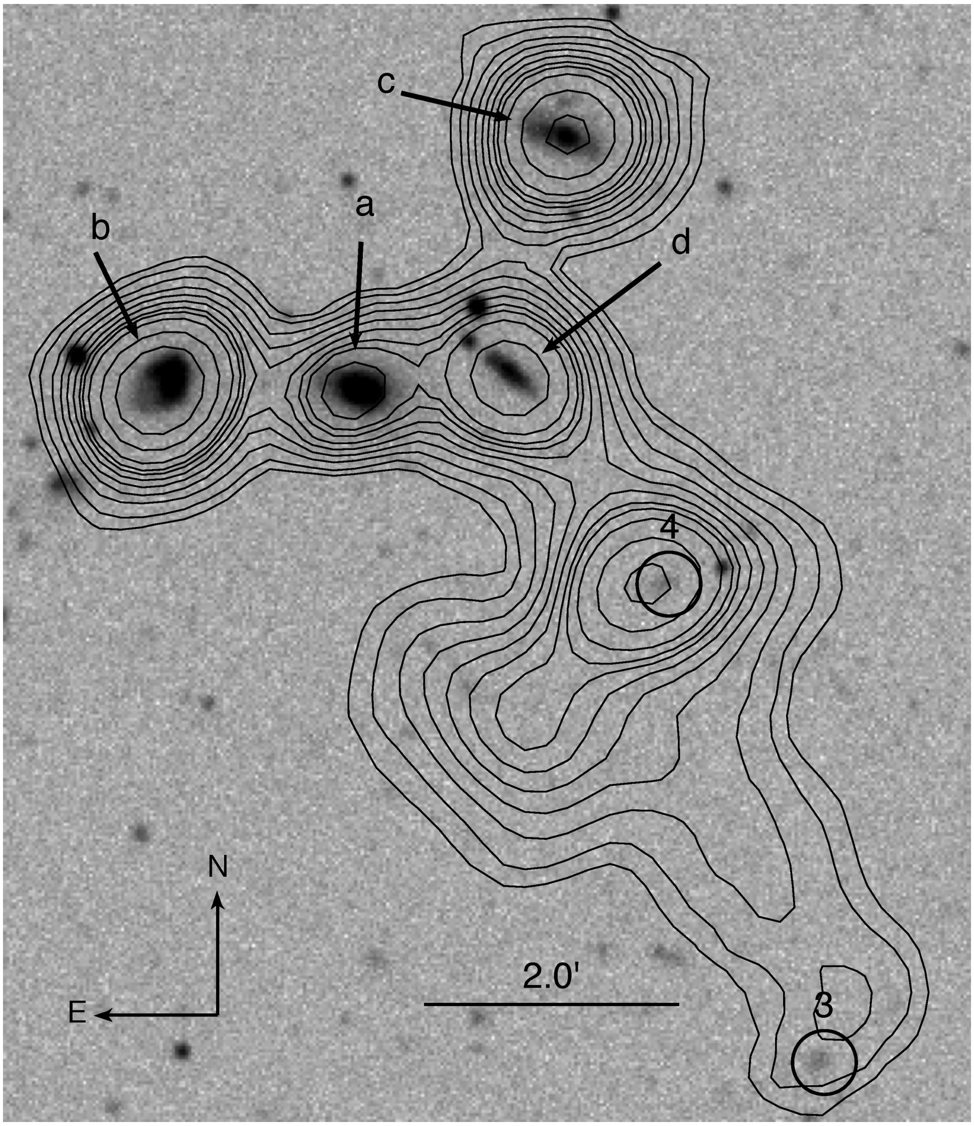

Figure 2. NUV image of HCG 100 where galaxy members a, b, c and d are labelled. Two TDG candidates, #3 and #4, are marked. They fall within the H I tail as shown in de Mello et al. (2008a). North is up and East is to the left. Bar length is 2 arcmin. Very Large Array (VLA) NHI contours are 0.6, 1.2, 2.1, 3.6, 4.4, 5.1, 5.9, 6.6, 7.4 × 10^{20} cm^{-2}.

clusters close to T124, T117 and T122, are 7 and 50 Myr but are not resolved in the *GALEX* image and therefore are not part of our analysis. Another object, T118, is 125 Myr and has not passed our selection criteria (more details are given in Section 3). These four stellar clusters are within the optical tail which is estimated to have formed due to a close interaction between NGC 7318A and NGC 7319 ∼200 Myr ago (Renaud, Appleton & Xu 2010). Therefore, our data show that H I tails in these two compact groups, HCG 92 and HCG 100, are laboratories of star formation.

3 DISCUSSION

In order to explore whether the environment where the newly discovered stellar clusters and TDG candidates are located plays a significant role in their formation, we have analysed other interacting systems with extended H I tails using a sample of galaxies from the rogues gallery of H I maps of peculiar and interacting galaxies compiled by Hibbard et al. (2001).[3] We identified 25 interacting systems with *GALEX* data with exposure times >1 ks which have also been observed by the Sloan Digital Sky Survey. We followed the same method to identify UV sources and to obtain their ages as we did for the compact groups. Since we are looking for young regions predominately composed of the luminosity of O, B and A stars, we defined a conservative cut in age at 100 Myr. We note that all new objects reported in the previous section for HCG 92 and HCG 100 are within this age range. We have also adopted a cut in luminosity equivalent to 100 O 8V stars ($100 \times L_{\rm FUV} = 100 \times 2 \times 10^{37}$ erg s^{-1}) or 4.2×10^{39} erg s^{-1}. This limit was set based on the luminosities of stellar clusters found in the H I bridge of M81 and M82 (also known as 'blue blobs') from de Mello et al. (2008b).

Six of the 25 interacting systems originally selected have 35 UV sources with ages < 100 Myr and luminosities higher than 4.2×10^{39} erg s^{-1} inside the H I contours. A description of each of these

---

[3] http://www.nrao.edu/astrores/HIrogues/RoguesLiving.shtml

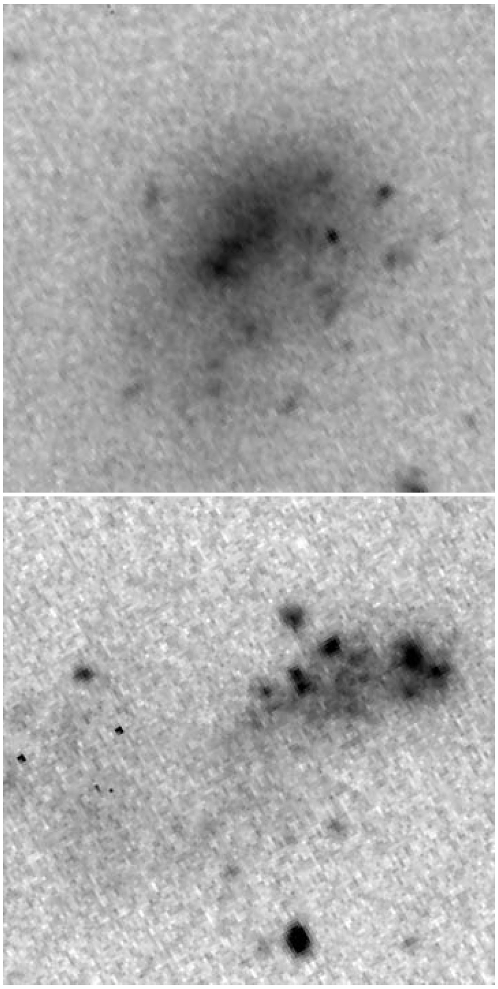

Figure 3. Gemini image (filter *r*) of the two TDG candidates in the H I tail of HCG 100 as originally identified in de Mello et al. (2008a) as objects #3 (top) and #4 (bottom). North is up and East is to the left.

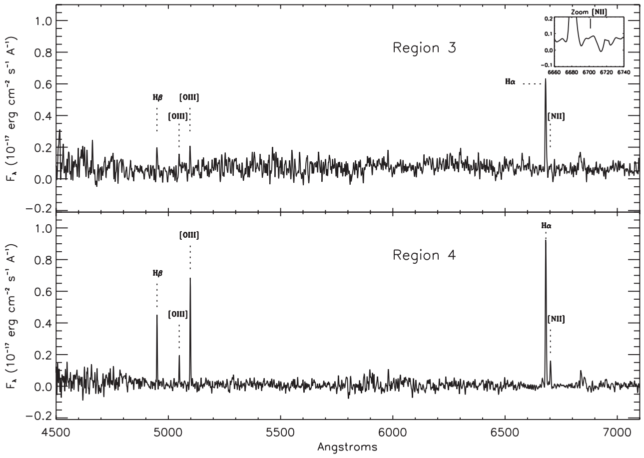

Figure 4. Spectra of HCG 100's regions 3 (top) and 4 (bottom) identified in de Mello et al. (2008a). These spectra were taken with B600 and R400 gratings. The marked lines were used to estimate the oxygen abundance (12+log(O/H)). A zoom into the Hα line region is shown on the right-hand side of the top figure.

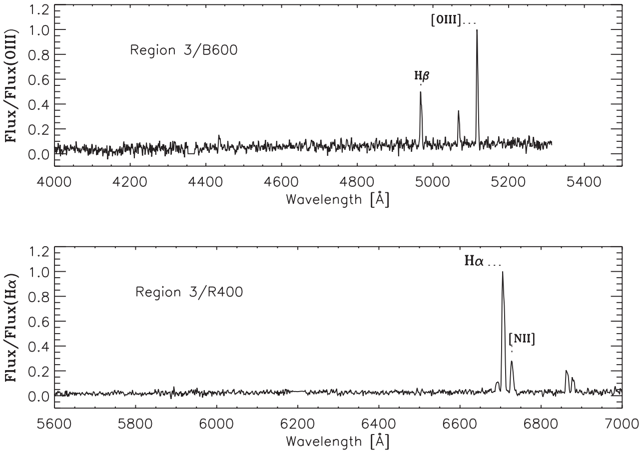

Figure 5. Spectra of HCG 92's region 3. Spectra taken with B600 grating are in the top panel and with R400 are in the bottom one. The marked lines were used to estimate the metallicities (12+log(O/H)). These spectra were not flux calibrated, given that no calibration star was available.

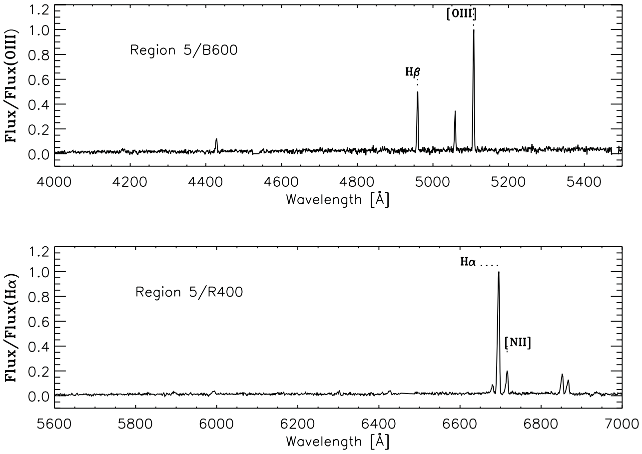

Figure 6. Spectra of HCG 92's region 5. Spectra taken with B600 grating are in the top panel and with R400 are in the bottom one. The marked lines were used to estimate the metallicities (12+log(O/H)). These spectra were not flux calibrated, given that no calibration star was available.

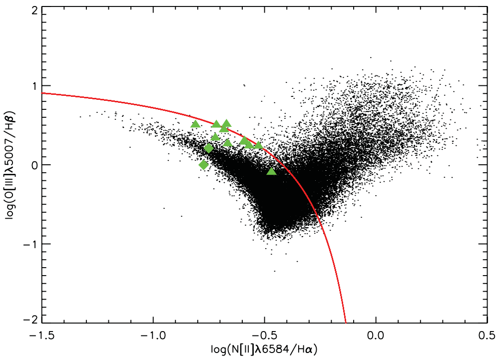

Figure 7. Line ratio diagram showing Sloan data from Kauffmann et al. (2003) and from star-forming regions in the H I tails of HCG 92 (triangles) and HCG 100 (diamonds). Objects with line ratios below the red line are classified as H II regions.

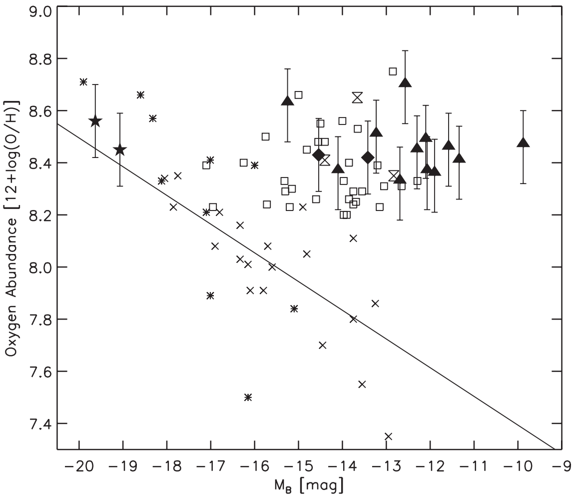

Figure 8. Absolute magnitude (M_B) versus oxygen abundance for local isolated dwarf galaxies (crosses), knots in tidal features (open squares), main group members (asterisk), main members HCG 100 (stars), H II region of Croxall et al. (2009, Hourglass) and our TDG candidates from HCG 92 (filled triangles) and HCG 100 (filled diamond). The line shows the correlation for dwarf galaxies from Weilbacher et al. (2003). The metallicities were obtained with the O3N2 index for the majority of the regions. The N2 calibrator was obtained for only one region of HCG 92. Adapted from Weilbacher et al. (2003).

six interacting systems is given in the appendix (Section 4.1). In Table 2, we list the regions, their colours, ages and luminosities, assuming that they are at the distance of the parent galaxies. Figs 10–15 show the different systems with their H I contours and the marked UV sources. We cannot exclude the possibility that a few or various UV sources we selected might be unrelated to the interacting galaxies, i.e. might be chance alignments. However, this method, when applied to HCG 100 by de Mello et al. (2008a), selected two TDG candidates within the H I tail and several stellar clusters in M81/M82 (blue blobs; de Mello et al. 2008b). As shown in the previous section, our GMOS data reveal that these two TDG candidates are at the same redshift as the galaxy group. Therefore, these two multiwavelength studies show that this approach is successful in identifying UV sources which are either star-forming regions or TDGs related to the interacting systems with stripped H I gas.

In order to compare the properties of the 35 UV sources found outside interacting galaxies with the ones in HCG 92 and HCG 100, we have calculated their luminosities and searched for similarities in the two populations. In Fig. 9, we show the distribution of luminosities versus ages for the 35 regions and we verify that the population of intergalactic regions contains objects with luminosities as high as $\sim10^{42}$ erg s^{-1} and as low as $\sim10^{39}$ erg s^{-1}, our lower limit. It is possible that the large range in luminosities indicates that we are dealing with different families of objects, as suggested in Mendes de Oliveira et al. (2004). As seen in Fig. 9, most of the regions in our sample are not as luminous as TDG candidates found in compact groups (filled symbols), except for object 2 around NGC 3079 and object 1 around NGC 3719. If that is the case, interacting galaxies are more likely to host star clusters while compact groups are more likely to host TDGs, as can be seen in Fig. 9. The low-mass objects might be similar to the M81–M82 ‘blue blobs’ described above. The high-mass objects would then be the TDG candidates. The Kolmogorov–Smirnov probability test confirms that luminosities of stellar clusters in interacting systems are significantly different from the ones in compact groups (KS = 0.000 13), i.e. luminosities are lower in the former than in the latter. We have also calculated masses using SB99 (Column 8 in Table 2) and the same trend is verified.

Further spectroscopic observations of these regions, as we did for HCG 92 and HCG 100, are needed in order to confirm their membership and establish their metallicities. It is possible that the group environment is more conducive to TDG formation (or better said, TDG survival) than pairs and mergers. This is in agreement with the simulations by Bournaud & Duc (2006) where specific conditions such as low impact velocity ($v < 250\,\mathrm{km\,s^{-1}}$), prograde encounters and mass ratio up to 4:1 may lead to TDG formation. HCGs might harbour these conditions besides the possibility that group potential may be able to drive TDGs away from the nearby proximity of their progenitor galaxies.

4 SUMMARY

We presented new Gemini spectroscopy of 14 star-forming regions within the H I tails of HCG 92 and in HCG 100 confirming that they are at same redshifts of the groups. We estimated their metallicity and verified that they are metal rich with respect to typical dwarf galaxies. This is possibly due to the fact that they were formed from pre-enriched material found in the intragroup medium.

We analysed *GALEX* FUV and NUV data of a comparison sample of six interacting galaxies containing a total of 35 UV sources in the H I tails. These star-forming regions span a wide range of ages (<100 Myr) and luminosities (10^{39}–10^{42} erg s^{-1}). We compared their properties with those of the star-forming regions in the H I tails of HCG 92 and HCG 100. We concluded that they have on average lower luminosity than the ones in the H I tails of compact groups. We suggest that this may be an environmental effect, i.e. that compact groups of galaxies with tidal tails of H I are more likely to host more massive star-forming regions or TDGs than other interacting galaxies. Spectroscopy of these sources is needed to confirm that they are at the same redshift as the interacting galaxies and to establish their metallicities.

4.1 Appendix

We present the *GALEX*/FUV images of the six interacting systems with extended H I gas. The FUV sources with ages < 100 Myr and $L > 10^{39}$ erg s^{-1} are marked. The H I contours are adapted from Hibbard et al. (2001).

4.1.1 NGC 2623

NGC 2623, also known as Arp 243, is located at 76.1 Mpc (Hattori et al. 2004). Bournaud et al. (2004) and Hattori et al. (2004) classified this object as a merger in an advanced stage. Hibbard & Yun (1996) found that a large part of the H I gas is located far away from the stellar component of NGC 2623.

In our analysis, we detected two young UV sources in the western tail of NGC 2623, as shown in Fig. 10. One of them (region #1 in Fig. 5) seems to be associated with the giant H II region (which could be a TDG candidate) detected by Bournaud et al. (2004) in their Fabry–Perot study. The age of this region is only 3 Myr. Its mass is about five times the mean mass of the intergalactic H II regions of Mendes de Oliveira et al. (2004). We detect another young region, #2 (Fig. 10), within the H I contours of NGC 2623. Interestingly, this region is also detected in the Hα map shown in Bournaud et al. (2004). The detection in the narrow band image confirms that these

Table 2. UV sources (ages < 100 Myr) in H I tails of six interacting galaxies.

ID	ID_region	RA(J2000)	Dec. (J2000)	FUV−NUV[a]	Age (Myr)[b]	$L_{\rm FUV}$ (erg s^{-1})	Log(M_*)[c]
NGC 2623	1	129.583 4808	25.758 4667	−0.14 ± 0.16	$3.6\pm_{2}^{4}$	40.14	4.7
NGC 2623	2	129.580 5054	25.751 1082	0.03 ± 0.11	$32.7\pm_{3}^{5}$	40.61	6.6
NGC 3079	1	150.559 6161	55.637 8441	−0.43 ± 0.02	$1.0\pm_{4}^{1}$	40.52	4.3
NGC 3079	2	150.551 4526	55.588 0432	−0.21 ± 0.12	$3.0\pm_{5}^{2}$	39.23	3.6
NGC 3079	3	150.134 4757	55.608 3908	0.02 ± 0.04	$33.4\pm_{6}^{13}$	39.48	6.0
NGC 3079	4	150.502 6245	55.712 8906	−0.19 ± 0.14	$3.7\pm_{8}^{3}$	39.95	3.8
NGC 3079	5	150.472 4426	55.740 3946	−0.32 ± 0.13	$2.1\pm_{9}^{5}$	39.80	3.3
NGC 3079	6	150.509 4452	55.685 6461	−0.22 ± 0.21	$2.3\pm_{5}^{15}$	40.31	3.8
NGC 3359	1	161.522 2015	63.147 3923	−0.26 ± 0.21	$2.7\pm_{8}^{2}$	40.70	4.3
NGC 3359	2	161.530 4108	63.160 9001	−0.13 ± 0.20	$3.7\pm_{1}^{4}$	39.65	3.5
NGC 3359	3	161.503 3569	63.221 5042	−0.30 ± 0.18	$2.4\pm_{6}^{2}$	39.92	3.5
NGC 3359	4	161.523 3002	63.234 6001	−0.09 ± 0.17	$4.2\pm_{8}^{6}$	41.02	5.0
NGC 3359	5	161.176 9409	63.100 1740	−0.23 ± 0.06	$2.9\pm_{2}^{7}$	39.63	3.2
NGC 3359	6	161.755 7220	63.262 3863	−0.25 ± 0.2	$2.5\pm_{5}^{2}$	39.64	3.2
NGC 3359	7	161.603 9429	63.281 5933	−0.16 ± 0.13	$3.3\pm_{4}^{8}$	39.66	3.4
NGC 3627	1	170.198 6084	12.969 6226	0.67 ± 0.08	$0.1\pm_{9}^{5}$	41.43	5.2
NGC 3718	1	173.254 8523	53.187 2864	0.14 ± 0.19	$84.5\pm_{3}^{14}$	41.57	7.2
NGC 3718	2	173.245 9717	53.157 1503	0.05 ± 0.27	$49.7\pm_{6}^{3}$	39.86	5.8
NGC 3718	3	173.222 4731	53.130 3406	−0.08 ± 0.06	$12.2\pm_{2}^{8}$	41.42	5.9
NGC 3718	4	173.207 1838	53.146 4157	0.05 ± 0.13	$49.5\pm_{9}^{4}$	40.38	5.7
NGC 3718	5	173.188 6292	53.159 5993	0.02 ± 0.12	$41.0\pm_{21}^{6}$	39.81	5.0
NGC 3718	6	173.144 6991	53.150 8026	−0.02 ± 0.17	$30.0\pm_{5}^{3}$	39.71	4.6
NGC 3718	7	173.017 4866	53.102 6154	0.11 ± 0.09	$71.8\pm_{7}^{2}$	40.42	6.0
NGC 3718	8	173.026 6724	52.991 7526	0.02 ± 0.18	$40.3\pm_{4}^{3}$	39.76	4.9
NGC 3718	9	173.167 4805	52.950 3860	0.13 ± 0.18	$79.9\pm_{3}^{1}$	39.62	5.3
NGC 3718	10	173.223 8617	53.039 7415	0.01 ± 0.14	$37.5\pm_{5}^{13}$	39.79	4.9
NGC 3718	11	173.076 0498	53.034 5230	0.05 ± 0.12	$48.7\pm_{6}^{14}$	39.91	5.2
NGC 4656	1	191.044 2352	32.262 8098	−0.05 ± 0.20	$3.8\pm_{1}^{14}$	40.55	4.4
NGC 4656	2	191.070 5109	32.271 0037	−0.09 ± 0.20	$10.8\pm_{5}^{23}$	40.01	5.1
NGC 4656	3	191.077 3621	32.275 5814	−0.10 ± 0.18	$2.5\pm_{12}^{4}$	39.79	3.4
NGC 4656	4	191.082 2449	32.287 6625	−0.24 ± 0.06	$1.8\pm_{15}^{5}$	40.22	3.7
NGC 4656	5	191.081 5887	32.280 7884	−0.26 ± 0.22	$1.3\pm_{2}^{7}$	39.68	3.3
NGC 4656	6	191.065 2161	32.291 9540	−0.07 ± 0.03	$13.8\pm_{8}^{6}$	39.83	5.1
NGC 4656	7	191.080 8105	32.306 8008	−0.31 ± 0.14	$1.0\pm_{4}^{2}$	40.13	3.8
NGC 4656	8	191.081 1768	32.312 0995	−0.09 ± 0.13	$2.5\pm_{6}^{1}$	39.82	3.4

[a] FUV and NUV magnitudes and errors were obtained using the IRAF task PHOT (Poisson). The errors in the colours were calculated using the magnitude errors added in quadrature.
[b] Age (Myr) estimated from the FUV−NUV colour.
[c] Stellar mass ($M_\odot$) obtained from SB99 monochromatic luminosity, L_{1530} (erg s^{-1}Å^{-1}), for the ages given in column 6.

two regions belong to the NGC 2623 system. In Table 2, we list the main physical parameters for each object.

4.1.2 NGC 3079

NGC 3079 is a giant spiral galaxy with two companions, MCG 9-17-9 (northeast) and NGC 3073 (southeast). NGC 3079 is located at 15 Mpc (de Vaucouleurs et al. 1991) and it is a type 2 Seyfert/low-ionization nuclear emission-line region with X-ray emission (Irwin & Saikia 2003; Kondratko, Greenhill & Moran 2005). This galaxy is one of the brightest observed mergers (Henkel et al. 1984). NGC 3073 is a dwarf galaxy with an elongated H I tail aligned with the core of NGC 3079.

We found six UV sources (Fig. 11) in this system. One of them seems to be associated with the H I contours of NGC 3073. In Table 2, we list the main physical parameters for each object.

4.1.3 NGC 3359

NGC 3359 is a barred spiral galaxy with several spiral arms and an irregular morphology in the outer parts of the disc.

NGC 3359 is at 13.4 Mpc (Rozas 2008) and it shows strong arms in the UV which are not observed in the optical. We detected seven UV sources (Fig. 12) in this peculiar spiral, plus one UV source in the isolated H I cloud far from the disc (region 5).

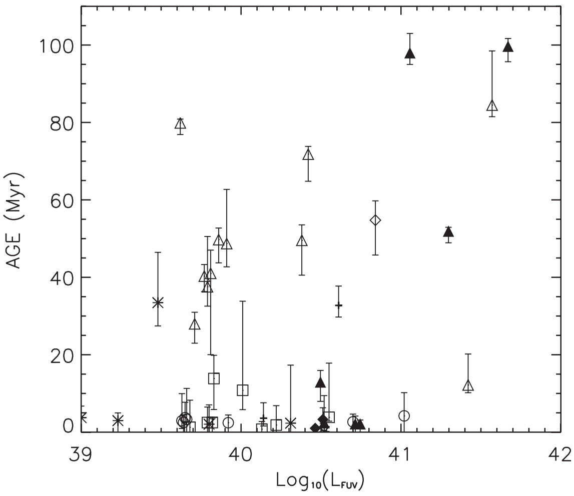

Figure 9. FUV luminosity (erg s^{-1}) versus age (Myr) for star-forming regions outside galaxies in six interacting galaxies (different symbol), HCG 100 (filled diamond) and HCG 92 (filled triangles).

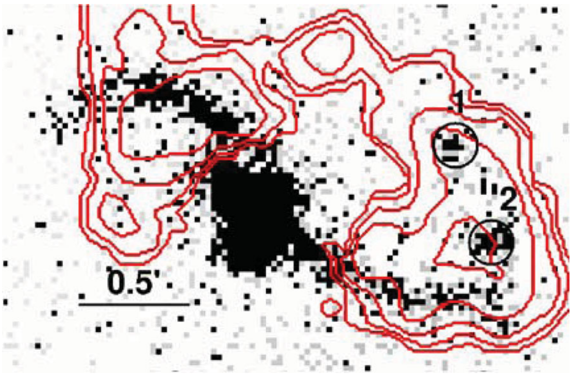

Figure 10. FUV image of NGC 2623, regions with ages < 100 Myr are marked with circles of 6 arcsec radius. H I contours = 4×10^{19} cm^{-2} $\times 2^n$ are from the VLA C+D-array and provided by Hibbard et al. (2001).

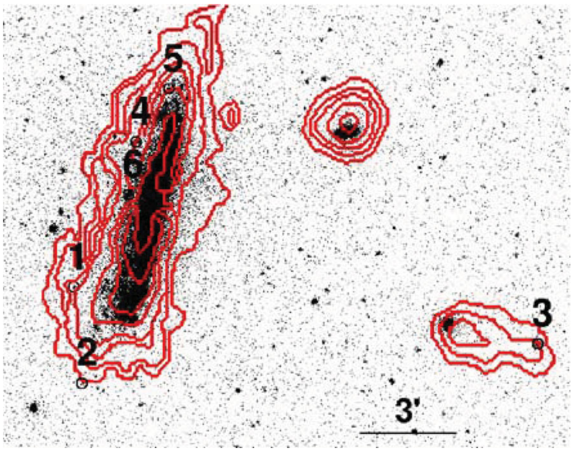

Figure 11. FUV image of NGC 3079; regions with ages < 100 Myr are marked with circles of 10 arcsec radius. NGC 3073 is a weak UV source close to source #3 in the figure. H I contours = (0.5, 1, 1.5, 2.4, 4, 10, 15, 25, 45) $\times 10^{20}$ cm^{-2} are from the VLA D-array and provided by Hibbard et al. (2001).

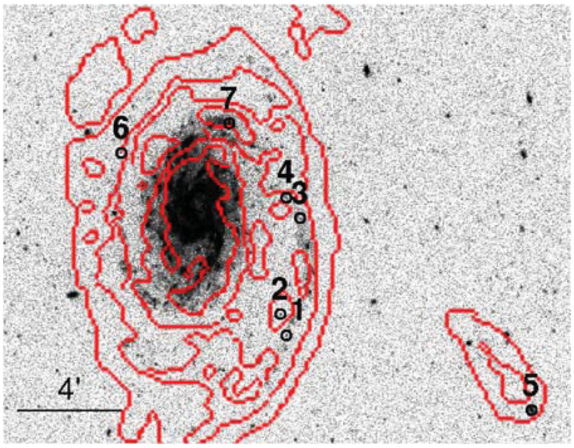

Figure 12. FUV image of NGC 3359; regions with ages < 100 Myr are marked with circles of 11 arcsec radius. H I contours = 3×10^{19} cm^{-2} $\times$ 2^n are from WSRT (30 arcsec resolution). The most outer contour is 5×10^{18} cm^{-2} for 60 arcsec resolution, and provided by Hibbard et al. (2001).

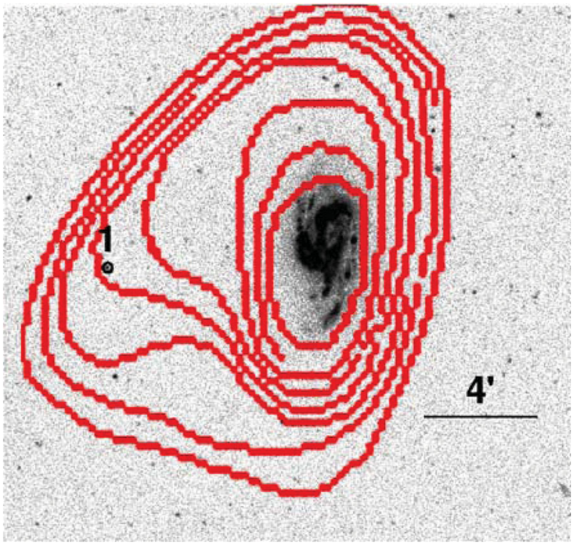

Figure 13. FUV image of NGC 3627; regions with ages < 100 Myr are marked with circles of 8 arcsec radius. H I contours = (3, 5, 10, 15, 25, 50, 75, 100, 200, 400, 600) K km s^{-1} are from Arecibo and provided by Hibbard et al. (2001).

4.1.4 NGC 3627

NGC 3627 is part of the Leo Triplet together with NGC 3623 and NGC 3628. The system is located at 6.7 Mpc (de Vaucouleurs 1975) and contains a remarkable H I bridge and a tail which can be due to an encounter between the galaxies in the past.

Here we present the results (Table 2) only for NGC 3627 (Fig. 13) since the other members are outside the *GALEX* field of view. We find only one UV source within the H I contour located close to the point where H I seems to peak.

4.1.5 NGC 3718

NGC 3718 is part of the Great Bear group and it is at 17 Mpc (Tully 1988). This galaxy has a peculiar morphology, showing strong dust lanes and diffuse/peculiar spiral arms. It has a large extension of H I gas, far from the optical disc (Allsopp 1979).

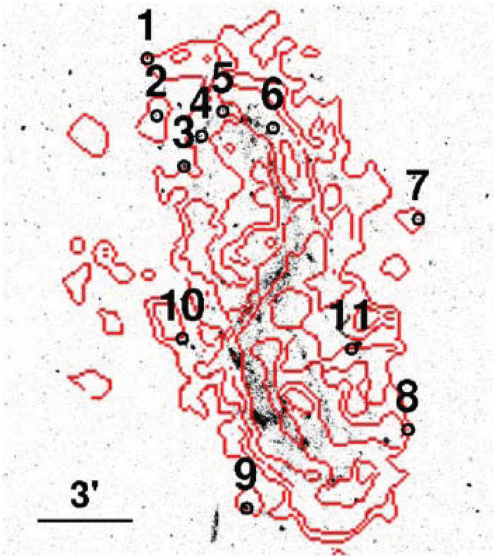

Figure 14. FUV image of NGC 3718; region with age < 100 Myr is marked with circle of 10 arcsec radius. H I contours $= 2 \times 10^{20}$ cm^{-2} $\times 2^n$ are from WSRT and provided by Hibbard et al. (2001).

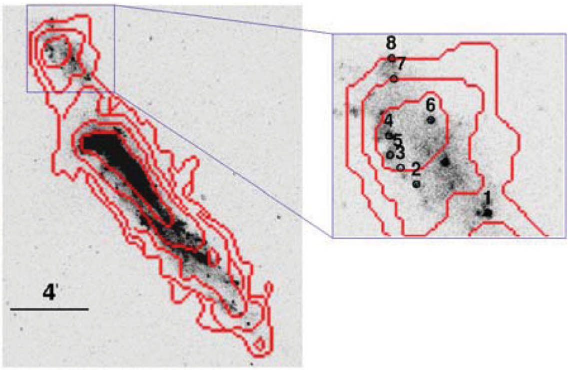

Figure 15. FUV image of NGC 4656, and a zoom of the candidate to TDG; the regions with ages < 100 Myr are marked with circles of 4 arcsec radius. H I contours $= 2 \times 10^{19}$ cm^{-2} $\times 2^n$ are from WSRT and provided by Hibbard et al. (2001).

NGC 3718 has 11 UV sources within the H I contour in both arms of the galaxy and outside the R_{25} optical radius (Fig. 14, Table 2).

4.1.6 NGC 4656

NGC 4656 is a spiral galaxy (Sc) interacting with NGC 4631 (Roberts 1968). They are linked by an H I bridge and are at 7.5 Mpc (Hummel, Sancisi & Ekers 1984). The bright region to the North of NGC 4656 resembles a TDG in the process of formation. We detected eight UV sources in this area (Fig. 15 and Table 2).

ACKNOWLEDGMENTS

We are grateful to an anonymous referee for helpful comments and suggestions. DFdM was funded by NASA Research grants NNG06GG45G and NNG06GG59G. FU-V acknowledges the financial support of FAPESP through an M.Sc. Fellowship, under contract 2007/06436-4. CMdO acknowledges support from Brazilian agencies FAPESP (projeto temático 2006/56213-9), CNPq and CAPES. STDF acknowledges the financial support of FONDECYT (Chile) through a post-doctoral position, under contract 3110087, and FAPESP through the Doctoral position, under contract 2007/07973-3. This research has made use of the NASA/IPAC Extragalactic Database (NED) which is operated by the Jet Propulsion Laboratory, California Institute of Technology, under contract with the National Aeronautics and Space Administration. Some of the data presented in this paper were obtained from the MAST. STScI is operated by the Association of Universities for Research in Astronomy, Inc., under NASA contract NAS5-26555. Support for MAST for non-*HST* data is provided by the NASA Office of Space Science via grant NAG5-7584 and by other grants and contracts.

REFERENCES

Allsopp N. J., 1979, MNRAS, 186, 343
Baldwin J. A., Phillips M. M., Terlevich R., 1981, PASP, 93, 5
Bertin E., Arnouts S., 1996, A&AS, 117, 393
Bianchi L. et al., 2007, ApJS, 173, 659
Bournaud F., Duc P.-A., 2006, A&A, 456, 481
Bournaud F., Duc P.-A., Amram P., Combes F., Gach J.-L., 2004, A&A, 425, 813
Chabrier G., 2003, PASP, 115, 763
Cortese L., Boselli A., Franzetti P., Decarli R., Gavazzi G., Boissier S., Buat V., 2008, MNRAS, 386, 1157
Croxall K., van Zee L., Lee H., Skillman E. D., Lee J. C., Côté S., Kennicut R. C., Jr, Miller B. W., 2009, AJ, 705, 72
de Mello D. F., Torres-Flores S., Mendes de Oliveira C., 2008a, AJ, 135, 319
de Mello D. F., Smith L. J., Sabbi E., Gallagher J. S., Mountain M., Harbeck D. R., 2008b, AJ, 135, 548
de Vaucouleurs G., 1975, ApJ, 202, 319
de Vaucouleurs G. et al., 1991, Third Reference Catalogue of Bright Galaxies. Springer, New York
Fall S. M., Chandar R., Whitmore B. C., 2005, ApJ, 631, L133
Fedotov K., Gallagher S. C., Konstantopoulos I. S., Chandar R., Bastian N., Charlton J. C., Whitmore B., Trancho G., 2011, AJ, 142, 42
Gallagher S. C., Charlton J. C., Hunsberger S. D., Zaritsky D., Whitmore B. C., 2001, AJ, 122, 163
Hattori T. et al., 2004, AJ, 127, 736
Henkel C., Guesten R., Downes D., Thum C., Wilson T. L., Biermann P., 1984, A&A, 141, L1
Hibbard J., Yun M., 1996, in Bremer M. N., ed., Cold Gas at High Redshift. Kluwer, Dordrecht, p. 47
Hibbard J., van Gorkum J. H., Rupen M. P., Schiminovich D., 2001, in Hibbard J. E., van Gorkum J. H., Rupen M. P., eds ASP Conf. Ser. Vol. 240, Astron. Soc. Pac., San Francisco
Hibbard J. et al., 2005, ApJ, 619, L87
Hickson P., 1982, AJ, 255, 382
Hummel E., Sancisi R., Ekers R. D., 1984, A&A, 133
Iglesias-Páramo J., Vílchez J. M., 2001, 550, 204
Irwin J. A., Saikia D. J., 2003, MNRAS, 346, 977
Kauffmann G. et al., 2003, MNRAS, 341, 54
Kondratko P., Greenhill L., Moran J., 2005, ApJ, 618, 618
Leitherer C. et al., 1999, ApJS, 123, 3
Lisenfeld U. et al., 2008, AJ, 685, 181
Mendes de Oliveira C., Cypriano E. S., Sodré L., Jr, Balkowski C., 2004, ApJ, L17
Mendes de Oliveira C., Temporin S., Cypriano E. S., Plana H., Amram P., Sodré L., Jr, Balkowski C., 2006, AJ, 132, 570
Moles M., Sulentic J. W., Marquez I., 1997, ApJ, 485, L69
Morrisey P. et al., 2005, ApJ, 619, L7
Mullan B. et al., 2011, ApJ, 731, 93
Neff S. G. et al., 2005, ApJ, 619, L91
Oosterloo R., Morganti R., Sadler E. M., Ferguson A., van der Hulst T., Jerjen H., 2004, in Duc P.-A., Braine J., Brinks E., eds, Proc. IAU Symp.

217, Recycling Intergalactic and Interstellar Matter. Astron. Soc. Pac., San Francisco, p. 486

Osterbrock D., Ferland G., 2006, Astrophysics of Gaseous Nebulae and Active Galactic Nuclei University Science Books, Sansalito

Pettini M., Pagel B. E. J., 2004, MNRAS, 348, L59

Renaud F., Appleton P. N., Xu C. K., 2010, ApJ, 724, 80

Richer M., McCall M., 1995, ApJ, 445, 642

Roberts M. S., 1968, ApJ, 151, 117

Rozas M., 2008, Rev. Mex. Astron. Astrofís., 44, 71

Ryan-Weber E. V. et al., 2004, AJ, 127, 1431

Schlegel D. J., Finkbeiner D. P., Davis M., 1998, ApJ, 500, 525

Seibert M. et al., 2005, ApJ, 619, L55

Sulentic J. W., Rosado M., Dultzin-Hacyan D., Verdes-Montenegro L., Trinchieri G., Xu C., Pietsch W., 2001, AJ, 122, 293

Thilker D. A. et al., 2007, ApJS, 173, 538

Thilker D. A. et al., 2009, Nat, 457, 990

Torres-Flores S., Mendes de Oliveira C., de Mello D. F., Amran P., Plana H., Epinat B., Inglesias-Paramo J., 2009, A&A, 507, 723

Torres-Flores S., Mendes de Oliveira C., de Mello D. F., Scarano S. J., Urrutia-Viscarra F., 2012, MNRAS, 421, 3612

Trancho G., Kostantopoulos I. S., Bastian N., Fedotov K., Gallagher S., Mullan B., Charlton J. C., 2012, ApJ, 748, 102

Tully R. B., 1988, Nearby Galaxies Catalog. Cambridge Univ. Press, Cambridge

Weilbacher P. M., Fritze-v., Alvensleben U., Duc P.-A., Fricke K., 2002, ApJ, 5795, 79

Weilbacher P. M., Duc P.-A., Fritze-v. Alvensleben U., 2003, A&A, 397, 545

Werk J. K. et al., 2011, ApJ, 678, 888

This paper has been typeset from a TEX/LATEX file prepared by the author.